Observation of high-temperature bubbles in an ECR plasma

K. Terasaka, S. Yoshimura and (iD) M. Y. Tanaka

View Online   Export Citation   CrossMark

ARTICLES YOU MAY BE INTERESTED IN

Observation of high-temperature bubbles in an ECR plasma

K. Terasaka,[1,a)] S. Yoshimura,[2] and M. Y. Tanaka[1]

[1]*Interdisciplinary Graduate School of Engineering Sciences, Kyushu University, Kasuga, Fukuoka 816-8580, Japan*
[2]*National Institute for Fusion Science, Toki, Gifu 509-5292, Japan*

Creation and annihilation of high-temperature bubbles have been observed in an electron cyclotron resonance plasma. The electron temperature in the bubble core is three times higher than that in the ambient region, and the size perpendicular to the magnetic field is much smaller than the plasma diameter. Formation of a bubble accompanies large negative spikes in the floating potential of a Langmuir probe, and the spatiotemporal behavior of the bubble has been visualized with a high-impedance wire grid detector. It is found that the bubble is in a prolate spheroidal shape with the axis along the magnetic field and occurs randomly in time and independently in space. *Published by AIP Publishing.* https://doi.org/10.1063/1.5027588

I. INTRODUCTION

Partially ionized plasma is a ubiquitous state of matter and is frequently found in nature. In the partially ionized plasmas, charge exchange interaction between ions and neutral particles is possible and a substantial amount of momentum is exchanged in this interaction, which is called the Sena effect.[1] Plasma ions and neutral particles couple with each other, making a multi-fluid system, and play an important role in atmosphere-ionosphere coupling,[2] structure formation of ionosphere interacting with the upper atmosphere,[3] blob dynamics in laboratory plasmas,[4] and so on. We have observed a small scale temperature localization, referred to as a high temperature bubble, in an electron cyclotron resonance (ECR) plasma. The high temperature bubble is in an elongated-spheroidal shape, and repeats creation and annihilation in a random manner like the boiling process. The bubble structure accompanies a neutral depletion hole, and is generated through an interplay between ion and neutral particles, showing a multi-fluid aspect of partially ionized plasmas.

Recently, we have observed large negative spikes in the floating potential of a Langmuir probe immersed into an electron cyclotron resonance (ECR) plasma. This observation means that high energy electron clumps, which are referred to as *high-temperature bubbles*, are generated in the plasma. It has also been found that the bubble accompanies a neutral depletion hole, suggesting that the bubble structure is established through the interplay between plasma and neutrals. In this paper, we report spatiotemporal behavior of the bubble and its statistical property.

To study bubble formation in a plasma, a new diagnostic tool is needed to be developed, which visualizes the spatial profile of events randomly occurring in time. We have developed a high-impedance wire grid (HIWG) detector and reconstructed a cross-sectional view of the bubble, which is described in Sec. II as well as the experimental apparatus. The experimental results including cross-sectional views of

the bubble are given in Sec. III A. The three-dimensional (3D) shape of the bubble has been obtained by making time slices of the bubble and is found to be a prolate spheroid with the axis along the magnetic field.

The statistical property of the bubble has been examined by evaluating the Hurst exponent for the time series of the floating potential, and it has been found that the bubble events occur randomly in time. As for the spatial property of the bubble events, it has been found that the generation rate of the bubble is spatially uniform, and that occurrence of a bubble does not affect the generation of the subsequent bubbles, i.e., the bubble occurs independently in space, which is described in Sec. III B. In Sec. IV, we consider the bubble formation scenario, emphasizing the multi-fluid aspect of partially ionized plasma, and the conclusion is given in Sec. V.

II. EXPERIMENTAL METHOD

The experiments have been carried out with the high-density plasma experiment device (HYPER-I[5]) at the National Institute for Fusion Science. The HYPER-I device produces high density plasmas by ECR heating. Figure 1 shows a schematic diagram of the experimental setup. The
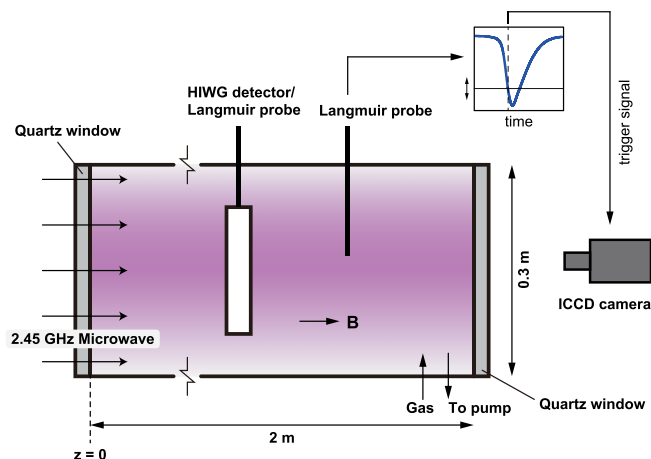

FIG. 1. Schematic diagram of the HYPER-I device.

a)terasaka@aees.kyushu-u.ac.jp

diameter and axial length of the vacuum vessel are 0.3 m and 2.0 m, respectively. Ten water-cooled magnetic coils are set around the vacuum chamber to make a weakly diverging magnetic field. A rectangular TE_{10} mode microwave with a frequency of 2.45 GHz is converted to a circular TE_{11} mode and further converted to a right-hand circular polarized mode by a circular polarizer. Then, the circular-polarized microwave is guided to the vacuum chamber through a tapered circular-waveguide and axially launched from an open end of the chamber. A right-hand circularly polarized mode (electron cyclotron wave) is excited in the plasma and absorbed in the ECR layer located in the middle of the chamber.

Electron cyclotron wave has a large absorption coefficient, and it has been experimentally confirmed that the region $0.65 < \omega/\omega_{ce} < 1.0$ (ω: frequency of microwave, ω_{ce}: electron cyclotron frequency) becomes an absorption layer.[6] Since a weakly diverging magnetic field configuration is adopted in the HYPER-I device, the plasma volume longer than 1 m in the axial direction becomes the absorption layer. A helium gas is used with operating pressures of 1.5 mTorr. The bubble formation has been observed with input power 5–25 kW. To obtain enough number of events in conditional sampling, we have carried out the experiments in high power conditions (20 kW).

Floating potential has been measured by a Langmuir probe. The diameter and the axial length of the probe tip are 1.5 mm and 1.0 mm, respectively. Since the magnitude of the floating potential signal is sensitive to the influx of high energy electron components, the large negative amplitude in the floating potential signal can be used as an indication of the existence of a high energy electron clump. The amplitude of the potential spike is utilized as a trigger threshold of the onset of bubble formation in conditional measurements with a Langmuir probe and an ICCD camera.

"Head-on" collisions of the bubble with respect to a reference Langmuir probe are chosen by magnitude of the floating potential signal, which is set to 12 times the standard deviation. A right-in-front image of the bubble has been obtained by accumulating emission intensity at 668 nm (He I) with an ICCD camera (Princeton Instrument ICCD 576 MG/1), which is triggered by the above-mentioned condition.

To visualize a cross-sectional view of the bubble, we have utilized the HIWG detector and reconstructed 2D cross-sectional image at an arbitrary instance of time. The HIWG detector consists of 8 horizontal and 8 vertical tungsten wires (0.8 mm in diameter), each of which is located with 10 mm spacing and electrically isolated. The HIWG detector outputs time traces of the floating potential signal from the 16 wires. The spatial structure has been reconstructed by making a contour map of the structure matrix $F(j, k)$, which is defined by geometrical means of floating potential values: $F(j, k) = \sqrt{\tilde{\phi}_j \times \tilde{\phi}_k}$, where $\tilde{\phi}_j$ and $\tilde{\phi}_k$ are the floating potential amplitudes of the j-th vertical wire ($j = 1$–8) and that of the k-th horizontal wire ($k = 1$–8), respectively. Figure 2 shows a case where a high-temperature bubble is present in the upper-right corner. The magnitude of the structure matrix $F(j, k)$ takes large values only when both the vertical and
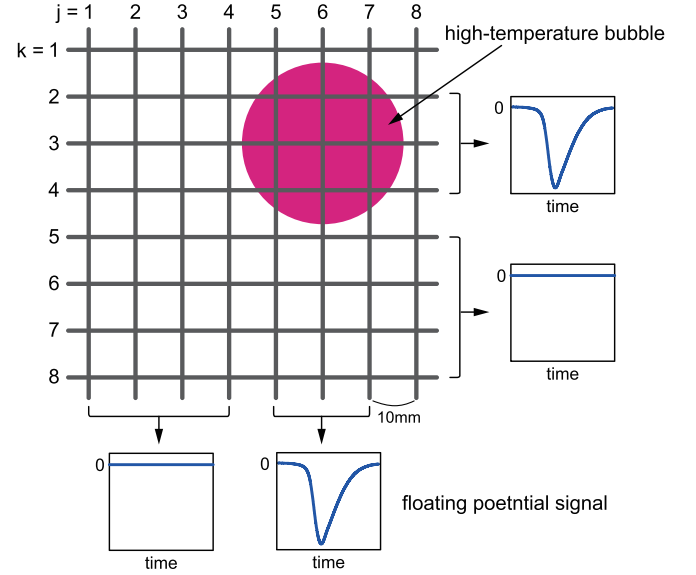

FIG. 2. Schematic diagram of the HIWG detector. Structure matrix $F(j, k)$ takes large values for $5 \leq j \leq 7$ and $2 \leq k \leq 4$, in this case. The contour map of the structure matrix exhibits spatial distribution of a high-temperature bubble.

horizontal wires simultaneously contact the high-temperature bubble. In the case depicted in Fig. 2, magnitudes of the structure matrix are large for the elements ($5 \leq j \leq 7$, $2 \leq k \leq 4$), and the other elements remain small because one of the potential magnitudes is small. The contour map of the structure matrix exhibits spatial profile of the high-temperature bubble. The size and occurrence position of the bubble have been determined from the contour map. The detailed description of the HIWG detector is presented in Ref. 7.

III. EXPERIMENTAL RESULTS

A. Observation of high-temperature bubbles

Figure 3(a) shows a time trace of floating potential of a Langmuir probe immersed in the plasma. As seen in the figure, there are many negative spikes on the trace, and magnitudes of potential change are larger than 20 V, where the quantities $\phi_0 = (1/N) \sum_i^N \phi_i$ and $S = [(1/N) \sum_i^N (\phi_i - \phi_0)^2]^{1/2}$ in the figure are the average value and the standard deviation of the floating potential signal, respectively. The Hurst exponent, H, which is a measure of randomness, is also shown in the figure (the Hurst exponent is explained in Sec. III B). The spike appears in the experimental conditions (1–3 mTorr of filling gas pressure and 5–25 kW of microwave input power), in which the electron pressure is comparable to that of neutral gas. In other discharge conditions, e.g., the lower gas pressure conditions,[8,9] the plasma is in the quiescent state. The enlarged views for various spike amplitudes are shown in Fig. 3(b), where more than 100 pulses with the same spike amplitude are accumulated and averaged after taking the time series. The duration of a single spike is about 5–10 μs, which is much longer than the electron time scale. We have also observed potential spike events in Ne, Ar, and Xe plasmas in the HYPER-I device, and the mean duration time of the spike event changes in proportion to the square root of atomic
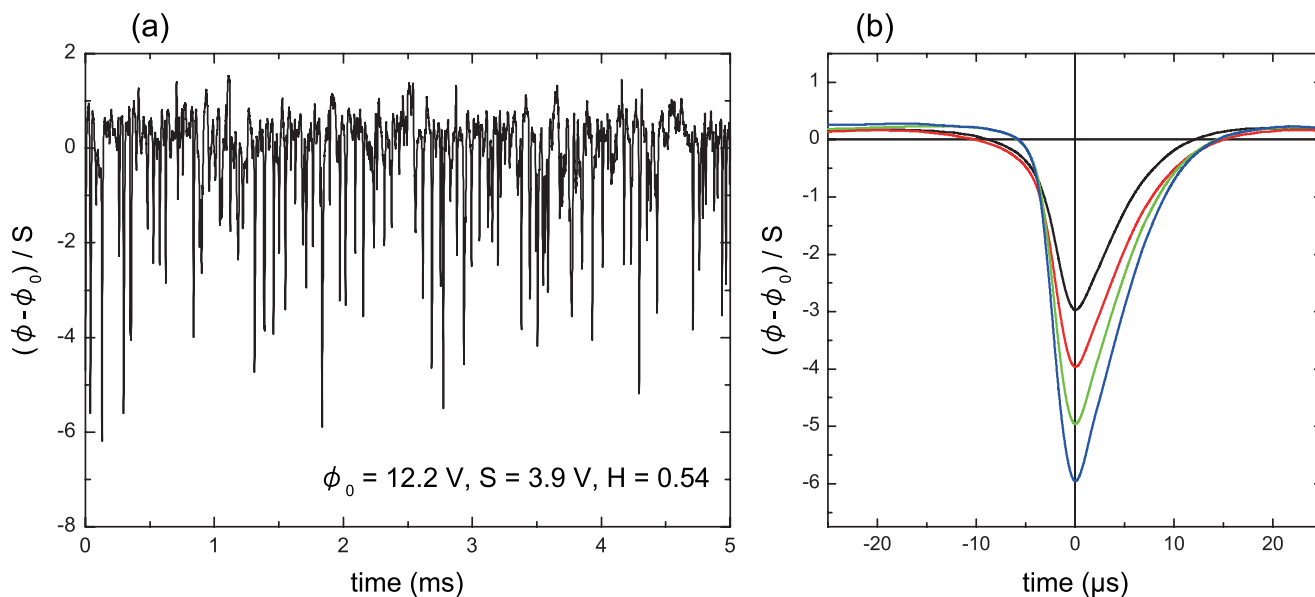
FIG. 3. Floating potential of a Langmuir probe. (a) Time trace of floating potential of a Langmuir probe immersed into a helium plasma, where the vertical axis indicates the normalized floating potential, $(\phi - \phi_0)/S$. The average value of floating potential is $\phi_0 = 12.2$ V, the standard deviation $S = 3.9$ V, and the Hurst exponent $H = 0.54$; (b) enlarged views of the spike event conditionally averaged over more than 100 pulses in each amplitude.

mass.[10,11] Furthermore, large negative spikes have also been found in the HYPER-II device,[12] indicating that the spike event is considered as a common nature in ECR plasmas.

Two-point Langmuir probe measurements show that the correlation between two floating potential signals at different positions vanishes with distance larger than 40 mm in the perpendicular direction with respect to the magnetic field, which indicates that the spike event is spatially localized in the plasma. Intensity of He I line emission at 668 nm accumulated under "head-on" events with respect to the reference probe is shown in Fig. 4. This image has been taken by the ICCD camera located at an open end of the chamber, where 120 events are collected and averaged. It is seen in the figure that there is a bubble structure with about 30 mm in diameter

in the plasma. The center of the bubble coincides with the tip of reference probe, which is imaged as a horizontal bar in the figure, and the high intensity region corresponds to the high temperature region.

To measure electron temperature in the bubble, we have taken the current-voltage (*I-V*) characteristic of a Langmuir probe immersed into the bubble, and compared with that outside the bubble. The *I-V* characteristic with the presence of bubble has been obtained with the conditional sampling method. The probe current is determined by averaging the same potential amplitude. By changing the bias voltage of the Langmuir probe, we have obtained the *I-V* characteristic at the bubble center and that in the peripheral point outside the bubble, which is shown in Fig. 5.

As seen in the figure, the electron temperature at the bubble center is 32 eV, and is three times higher than that in
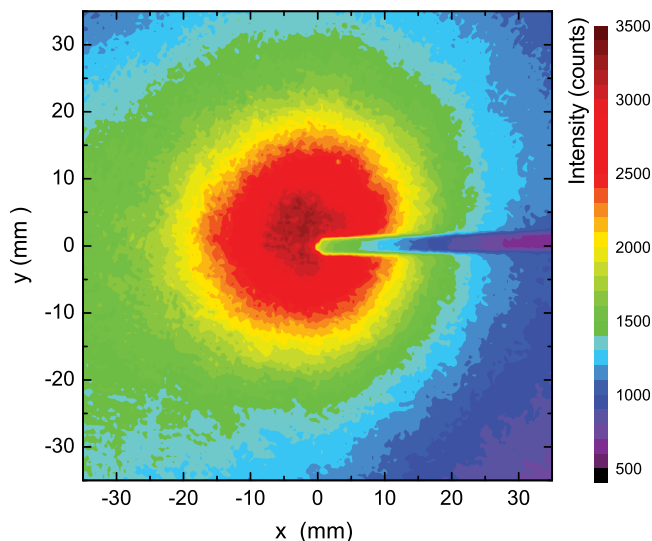

FIG. 4. 2D image of He I line emission (668 nm) taken by conditional operations of an ICCD camera. An image of the reference Langmuir probe (horizontal bar) is also shown in the figure.
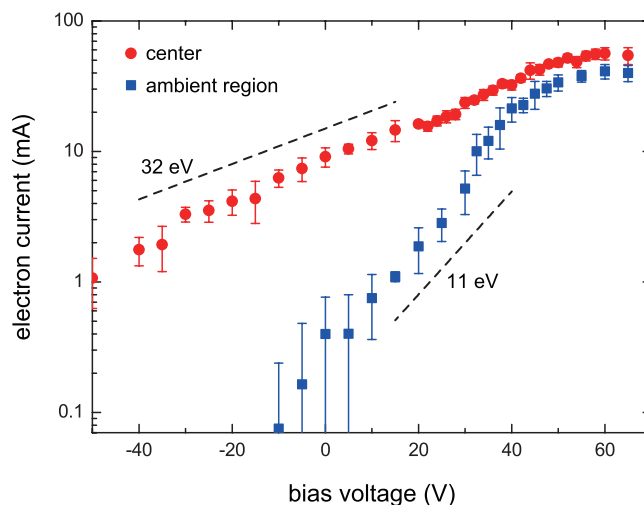

FIG. 5. Current-voltage characteristics of a Langmuir probe; closed circles: center of the bubble ($r = 0$ mm); closed squares: peripheral region ($r = 40$ mm).
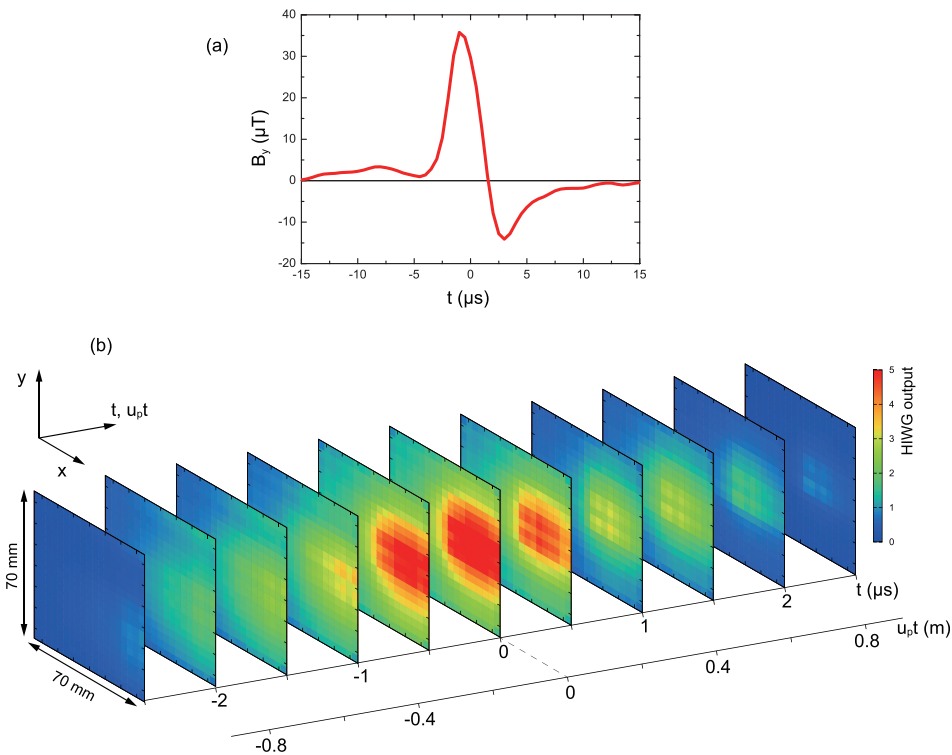
FIG. 6. Structure of the high-temperature bubble. Figure 6(a) shows time variation of the magnetic field measured with a magnetic probe and Fig. 6(b) shows the time slice of a high temperature bubble reconstructed with the HIWIG detector, where the spatial scale obtained by multiplying the propagation velocity (u_{p}) is also indicated.

the peripheral region (11 eV). Moreover, the central temperature exceeds the ionization energy of the operation gas species (He), indicating that neutral particles are expected to be more consumed in the bubble center than in the ambient region.

The high temperature bubble propagates along the magnetic field. Figure 6(a) shows the time variation of the perpendicular magnetic field component measured with a magnetic probe. From the two-point measurements, it has been found that the propagation velocity is $u_{\mathrm{p}} = 3.8 \times 10^5$ m/s, which agrees with the Alfvén velocity. The time axis of

the time-sliced figure is converted into spatial scale by multiplying the propagation velocity, which is shown in Fig. 6(b). The isosurface of Fig. 6(b) exhibits a spatial shape of the structure, showing a prolate spheroid with axis along the magnetic field. Figure 7 shows reconstruction images at 8 instants of time during a single discharge. Bubble events occur everywhere in the plasma cross section, and the plasma state under the bubble formation condition is considered as an ensemble of a single event randomly generated in the plasma. We have applied statistical analysis to the experimental data, which is described in Sec. III B.
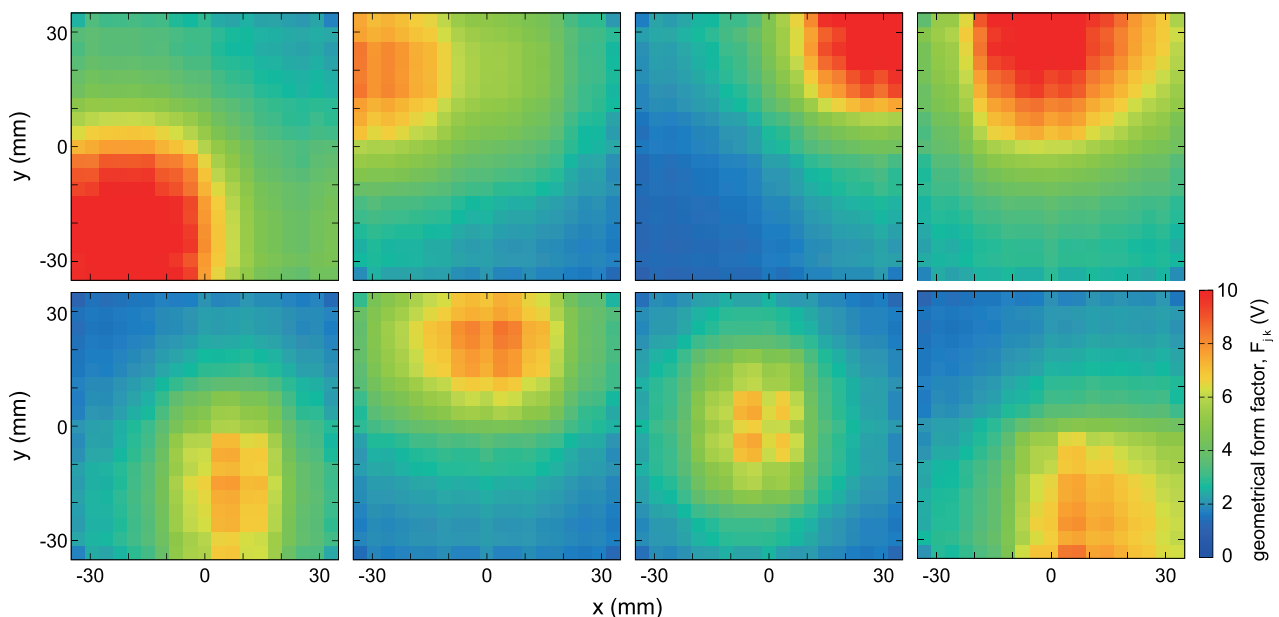

FIG. 7. Free running shots of bubble events reconstructed with the HIWG detector.

B. Statistical properties of bubble events

To examine the statistical properties of the bubble events, we have used the rescaled-adjusted range (RS) analysis[13,14] for the floating potential data to calculate the Hurst exponent. The Hurst exponent (denoted by H) is defined as an exponent of a quantity $R/S (\propto N^H)$, where the quantity R is the difference between the local maxima and minima of a subset of floating potential data with size N, and the quantity S is the standard deviation. When the Hurst exponent is greater than 1/2, the system has long time memory and behaves as persistent, when smaller than 1/2, the system behaves as anti-persistent and counter response to the previous state is likely to be realized. When events occur in a completely random manner, the Hurst exponent becomes 1/2.[15]

Figure 8 shows the radial profile of the Hurst exponent calculated from the floating potential data. The inset figure in Fig. 8 indicates the method for evaluating the Hurst exponent, which is determined in the region $N \geq 1000$. The Hurst exponent is spatially constant around $H = 1/2$, showing that the bubble generation temporally occurs in a random manner and that there is no singular point in the plasma as far as bubble generation is concerned. It has been reported by Yoshimura *et al.* that the probability density function for the waiting time of successive bubble events is well described by an exponential distribution over 3 decades (Ne, Ar, and Xe) to 4 decades (He) with respect to the waiting time.[10,11]

To examine the spatial characteristic of the bubble formation, we have evaluated the distribution of event rate in $10 \text{ mm} \times 10 \text{ mm}$ area during a 1.7 s time period. The total number of 10 166 events have been observed in the measurement period, for which the histogram of the event number is shown in Fig. 9(a). As seen in the figure, the number of events at each position is 180 to 320, and there is no singular point in the measured plasma cross-section. We have also evaluated the event rate as a function of distance between successive bubble events, and the results are shown in Fig. 9(b). The probability density of the event rate is almost constant with respect to the distance between successive two
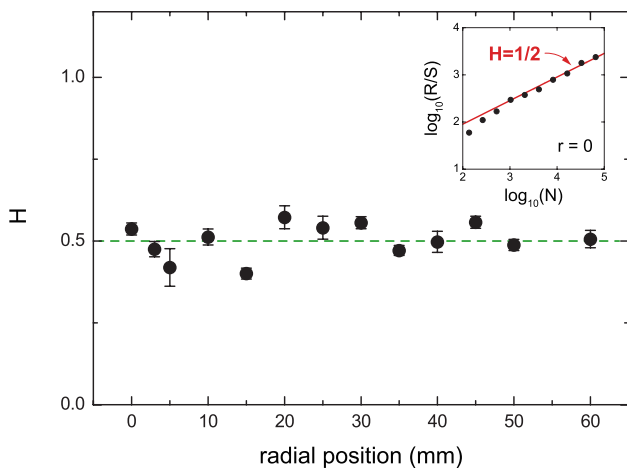

FIG. 8. Radial profile of the Hurst exponent evaluated from the floating potential data. The inset figure in the upper-right is the R/S as a function of the data size, N, at the center of plasma ($r = 0$ mm). The Hurst exponent is evaluated for $N \geq 1000$.
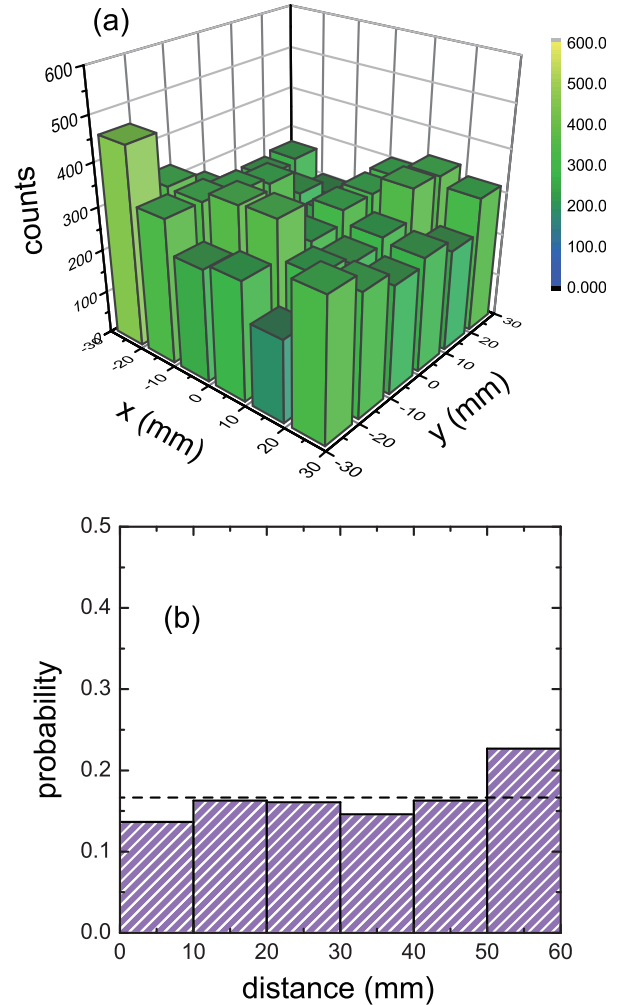

FIG. 9. Spatial property of the bubble events. (a) 2D distribution of the event rate during 1.7 s; (b) probability density as a function of distance between two consecutive events. The dashed line in (b) indicates the expected value for isotropic and random excitation case.

events, and is almost equal to the expected value for the random excitation case (broken line). We can conclude that occurrence of a bubble does not affect formation of the subsequent bubbles. According to the results on the statistical property, we can conclude that the bubble formation takes place randomly in time and independently in space. As far as bubble formation is concerned, the plasma behaves as a uniform medium.

IV. DISCUSSIONS

We have observed large negative spikes in the floating potential signal of a Langmuir probe immersed in an ECR plasma. It has been revealed that the spike events coincide with the generation of high-temperature bubbles with a few centimeters in diameter and that the bubble event randomly takes place in the plasma.

As seen in Fig. 5, electron temperature at the bubble center exceeds the ionization threshold of helium atoms (24.6 eV). In this condition, the helium neutral particles inside the bubble region are more consumed by ionization than in the low temperature peripheral region. From the

estimation with isotropic Maxwellian distribution of electrons, the contribution of ionization collision inside the bubble ($T_e = 30$ eV) is 2–3 times larger than that in the peripheral region ($T_e = 10$ eV), and the ionized neutral particles are exhausted as ions along the magnetic field.

In fact, neutral density distribution determined from He I line intensity ratio exhibits a neutral depletion hole as shown in Fig. 10, where the neutral density profile is evaluated from the 2D He I emission profile presented in Fig. 4 by using the electron temperature and density profiles. So far, the neutral depletion structure with a large size comparable to the plasma diameter has been observed in RF and helicon plasma sources.[16–18] However, a small depletion hole with a size of the bubble diameter has been first observed in the present experiment.

The experimental results give us an insight into the bubble formation scenario. Since the absorption coefficient of ECR heating depends on the plasma density, inhomogeneous heating may take place due to density perturbation. When the electron temperature inside the bubble happens to start increasing, neutral particles within the bubble are more ionized and exhausted as ions along the magnetic field. Consequently, neutral density in the bubble region further decreases to make a depletion hole. Since a decrease in neutral density diminishes dissipation of microwave energy, the electron temperature in the bubble region continues to increase. There is a positive feedback mechanism in electron temperature, which comes from the interplay between plasma and neutral particles. This feedback mechanism acts on plasma (electrons) until the depletion hole is filled with the recovery of ambient neutrals.

The size of the bubble is estimated by the expansion velocity (ion sound velocity) and the lifetime of the bubble, $C_s \times t_d$, where the quantity C_s is the ion sound velocity [1×10^4 m/s ($T_e = 10$ eV)] and the quantity t_d is the characteristic lifetime of the bubble, which is determined by the exponent of the time trace of the floating potential signal ($3\,\mu$s in the present experiment). Then, the expected bubble size is evaluated to be 30 mm in diameter.
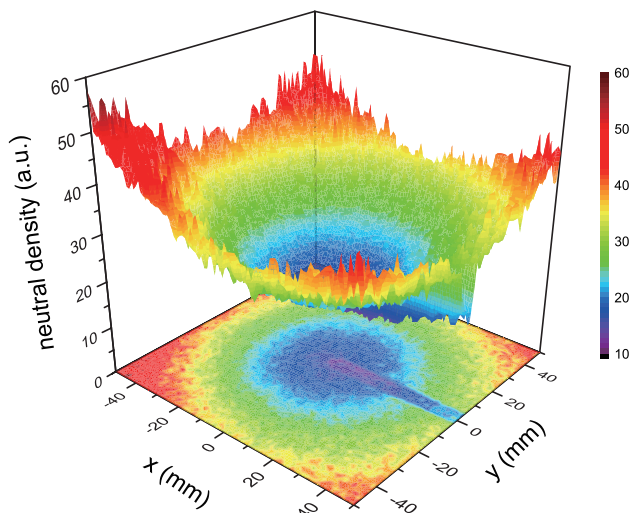
We have collected 149 bubble events and plotted the size distribution in Fig. 11. The mean values in the x-direction (X_W) and in the y-direction (Y_W) are $X_W = 30.3 \pm 4.7$ mm and $Y_W = 29.5 \pm 5.4$ mm, respectively. Figure 11 shows that the observed bubble sizes distribute around the expected value.

It is worth pointing out that the size of the neutral depletion hole is determined by the ionization mean free path or charge exchange mean free path, whichever is shorter. In the present experiment, the mean free path of charge exchange collision between ions and neutrals is shorter than that of ionization collision between electrons and neutrals. As a result, the scale of depletion hole accompanied with the bubble is governed by charge exchange collision in the present conditions. The mean free path and the collision time of charge exchange collision are estimated as 80 mm and 10 μs, respectively, and these values agree with the observations. This means that bubble generation is established through the interplay between ions and neutrals.

In partially ionized plasmas, a change in the plasma fluid induces a change in the neutral fluid. Two fluids affect each other to make a spatiotemporal structure. The response times of plasma (electrons) and neutral particles are much different, and hence the structure established in the plasma inevitably becomes dynamic, consisting of fast response of plasma (electrons) and slow recovery of neutrals.

The bubble in the plasma is initially created by fast electron heating and then annihilated with slow recovery of neutrals. It is considered as a coupled entity of temperature localization and "burnout" structure of background neutrals. According to the repetitive nature of events and randomness in occurrence, we can conclude that the formation of the bubble is considered as a kind of boiling process in a plasma.

Vortex is a well known entity that has an important role in mass and momentum transport in plasmas. We have found in these experiments that, in a partially ionized plasma, there is one more entity that plays an important role in transport,
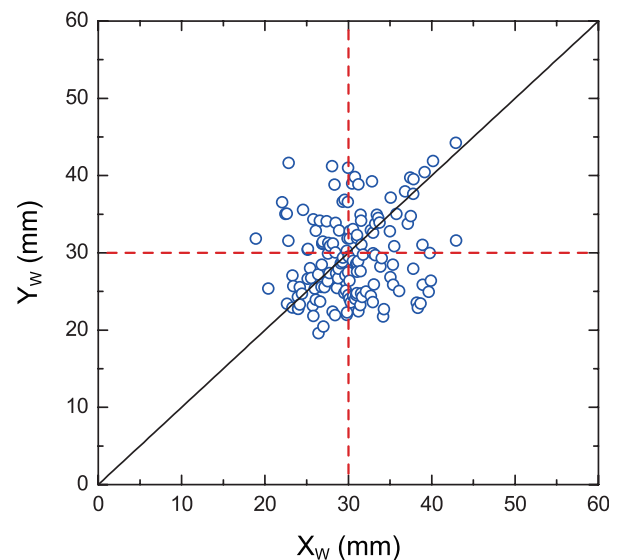

FIG. 10. Neutral depletion hole associated with a bubble.

FIG. 11. Distribution of bubble size. The size of the bubble is determined by full width at half maximum of the HIWG images. The sizes in the x-direction (X_W) and in the y-direction (Y_W) for 149 events are plotted by open circles. The expected bubble sizes are indicated by broken lines.

i.e., bubbles. A detailed study is an important issue for future work of fundamental plasma physics.

V. CONCLUSION

We have observed high-temperature bubbles in an ECR plasma. The shape of the bubble has been visualized with the HIWG detector and found that the bubble is a prolate spheroid with the axis along the magnetic field. By using the conditional averaging technique, we have found that the electron temperature in the bubble center exceeds the ionization energy of neutral atoms and that a neutral depletion hole is established inside the bubble. Statistical analysis has revealed that, as far as bubble formation is concerned, the plasma behaves as a uniform medium. The bubble phenomenon originates from the interplay between plasma and neutral fluids, and exhibits a multi-fluid aspect of partially ionized plasmas.

ACKNOWLEDGMENTS

[1] B. M. Smirnov, *Physics of Ionized Gases* (Wiley-VCH, Weinheim, 2004), pp. 164–176.

[2] T. Iyemori, M. Nose, D. Han, Y. Gao, M. Hashizume, N. Choosakul, H. Shinagawa, Y. Tanaka, M. Utsugi, A. Saito, H. McCreadie, Y. Odagi, and F. Yang, Geophys. Res. Lett. **32**, L20807, https://doi.org/10.1029/2005GL024083 (2005).

[3] H. Kil, J. Astron. Space Sci. **32**, 13 (2015).

[4] S. I. Krasheninnikov and A. I. Smolyakov, Phys. Plasmas **10**, 3020 (2003).

[5] S. Yoshimura, K. Terasaka, E. Tanaka, M. Aramaki, A. Okamoto, K. Nagaoka, and M. Y. Tanaka, J. Plasma Phys. **81**, 345810204 (2015).

[6] M. Tanaka, R. Nishimoto, S. Higashi, N. Harada, T. Ohi, A. Komori, and Y. Kawai, J. Phys. Soc. Jpn. **60**, 1600 (1991).

[7] K. Terasaka, S. Yoshimura, Y. Kato, K. Furuta, M. Aramaki, T. Morisaki, and M. Y. Tanaka, Rev. Sci. Instrum. **85**, 113503 (2014).

[8] K. Nagaoka, A. Okamoto, S. Yoshimura, M. Kono, and M. Y. Tanaka, Phys. Rev. Lett. **89**, 075001 (2002).

[9] K. Terasaka, S. Yoshimura, K. Ogiwara, M. Aramaki, and M. Y. Tanaka, Phys. Plasmas **17**, 072106 (2010).

[10] S. Yoshimura, K. Terasaka, E. Tanaka, M. Aramaki, and M. Y. Tanaka, Plasma Fusion Res. **10**, 3401028 (2015).

[11] S. Yoshimura, K. Terasaka, E. Tanaka, M. Aramaki, and M. Y. Tanaka, Jpn. Phys. Soc. Conf. Proc. **1**, 015030 (2014).

[12] K. Terasaka, M. Y. Tanaka, S. Yoshimura, M. Aramaki, Y. Sakamoto, F. Kawazu, K. Furuta, N. Takatsuka, M. Masuda, and R. Nakano, J. Plasma Phys. **81**, 345810101 (2015).

[13] H. E. Hurst, Trans. Am. Soc. Civil Eng. **116**, 770 (1951).

[14] H. E. Hurst, Nature **180**, 494 (1957).

[15] B. A. Carreras, B. Ph. van Milligen, M. A. Pedrosa, R. Balbin, C. Hidalgo, D. E. Neuman, E. Sánchez, M. Frances, I. Garcia-Cortés, J. Bleuel, M. Endler, C. Riccardi, S. Davies, G. F. Matthews, E. Martines, V. Antoni, A. Latten, and T. Klinger, Phys. Plasmas **5**, 3632 (1998).

[16] A. Aanesland, L. Liard, G. Leray, J. Jolly, and P. Chabert, Appl. Phys. Lett. **91**, 121502 (2007).

[17] C. M. Denning, M. Wiebold, and J. E. Scharer, Phys. Plasmas **15**, 072115 (2008).

[18] K. Takahashi, Y. Takao, and A. Ando, Appl. Phys. Lett. **108**, 074103 (2016).